# Exploring Stratocumulus Cloud-Top Entrainment Processes and Parameterizations by Using Doppler Cloud Radar Observations

BRUCE ALBRECHT AND MING FANG

*Rosenstiel School of Marine and Atmospheric Science, University of Miami, Miami, Florida*

VIRENDRA GHATE

*Environmental Science Division, Argonne National Laboratory, Argonne, Illinois*

(Manuscript received 3 June 2015, in final form 19 October 2015)

ABSTRACT

Observations made at the Atmospheric Radiation Measurement (ARM) Program's Southern Great Plains (SGP) site during uniform nonprecipitating stratocumulus cloud conditions for a 14-h period are used to examine cloud-top entrainment processes and parameterizations. The observations from a vertically pointing Doppler cloud radar provide estimates of vertical velocity variance and energy dissipation rate (EDR) terms in the parameterized turbulent kinetic energy (TKE) budget of the entrainment zone. Hourly averages of the vertical velocity variance term in the TKE entrainment formulation correlated strongly ($r = 0.72$) with the dissipation rate term in the entrainment zone, with an increased correlation ($r = 0.92$) when accounting for the nighttime decoupling of the boundary layer. Independent estimates of entrainment rates were obtained from an inversion-height budget using the local time derivative and horizontal advection of cloud-top height together with large-scale vertical velocity at the boundary layer inversion from the European Centre for Medium-Range Weather Forecasts (ECMWF) reanalysis model. The mean entrainment rate from the inversion-height budget during the 14-h period was $0.74 \pm 0.15\,\mathrm{cm\,s^{-1}}$ and was used to calculate bulk coefficients for entrainment parameterizations based on convective velocity scale $w^*$ and TKE budgets of the entrainment zone. The hourly values of entrainment rates calculated using these coefficients exhibited good agreement with those calculated from the inversion-height budget associated with substantial changes in surface buoyancy production and cloud-top radiative cooling. The results indicate a strong potential for making entrainment rate estimates directly from radar vertical velocity variance and the EDR measurements.

## 1. Introduction

Stratocumulus clouds are a particularly important component of Earth's climate because of their large impact on the radiation budget. Uncertainties in their representation in global climate models contribute substantially to variances among models in their prediction of climate change (e.g., Bony and Dufresne 2005). These persistent clouds cover vast areas over the eastern subtropical oceans. They form beneath a capping thermodynamic inversion and are intimately tied to turbulence in the boundary layer (BL), which is forced primarily by surface buoyancy production, cloud-top radiative cooling, wind shear, and drizzle (Wood 2012). The properties of stratocumulus clouds are greatly affected by cloud-top entrainment process—the mixing of free-tropospheric air above the inversion with the turbulent cloudy air. Although the importance of entrainment in affecting cloud properties was realized early (Lilly 1968), the parameterization of entrainment for stratocumulus cloud is yet to be fully resolved (Wood 2012; Bretherton and Blossey 2014).

The first effort to understand cloud-top entrainment can be found in the classic work by Lilly (1968), in which a budget for turbulence kinetic energy (TKE) was applied to the whole BL. Subsequent treatments of entrainment rate closures considered the TKE budget of the inversion layer (e.g., Tennekes 1973; Tennekes and Driedonks 1981). More recently, substantial theoretical, modeling, and observational work has focused on the

*Corresponding author address*: Bruce Albrecht, Dept. of Atmospheric Sciences, Rosenstiel School of Marine and Atmospheric Science, University of Miami, 4600 Rickenbacker Causeway, Miami, FL 33149.
E-mail: balbrecht@rsmas.miami.edu

DOI: 10.1175/JAS-D-15-0147.1

application of a simplified TKE budget to relate entrainment rates to vertical velocity variance in the cloud-topped BL and the convective velocity scale $w^*$ (e.g., Nicholls 1984; Nicholls and Turton 1986; Bretherton et al. 1999; Lock et al. 2000).

Assumptions about the relationship between eddy dissipation rates and other sources and sinks of TKE were fundamental in simplification of the TKE budget by Lilly (1968); this assumption remains implicit in the $w^*$ parameterizations currently used in large-scale models. However, the assumptions central to this simplification have been largely untested. The general approach for evaluating entrainment rate parameterizations that depends on the strength of the turbulence and BL structure comes from studies using either aircraft observations (e.g., Nicholls and Turton 1986; Malinowski et al. 2013) or large-eddy simulation (LES) models (e.g., Deardorff 1980; Bretherton et al. 1999; Kurowski et al. 2009). From aircraft observations, entrainment rates can be estimated by using the turbulent fluxes of scalar variables just below the capping inversion and the jumps in those variables at the inversion (e.g., Nicholls and Turton 1986; Faloona et al. 2005; Haman et al. 2007; Gerber et al. 2013). Further, aircraft observations of the temporal and spatial variability of the inversion height (or the variability along Lagrangian flights) can be combined with large-scale model (reanalysis) estimates of the vertical velocity to provide additional estimates of entrainment rates (Stevens et al. 2003; Faloona et al. 2005) by using boundary layer mass budget formulations. Aircraft turbulence observations are used to obtain the vertical velocity variance and $w^*$. This general approach and the associated uncertainties in entrainment rates from aircraft observations are described in Faloona et al. (2005). In studies using LES models, simulations provide entrainment rates that can be related to the resolved vertical velocity variance and $w^*$ (e.g., Deardorff 1980; Bretherton et al. 1999). These observational and modeling approaches include an implicit assumption in simplification of the TKE budget so that the eddy dissipation rate is proportional to the vertical velocity variance. However, direct quantitative verification of this assumption is difficult to obtain from aircraft observations (Brost et al. 1982; Nicholls 1984).

The development and application of Doppler cloud radars has provided a means to characterize the turbulence structure in both marine (Frisch et al. 1995; Ghate et al. 2014; Lothon et al. 2005) and continental stratocumulus clouds (Kollias and Albrecht 2000; Ghate et al. 2010). One distinct advantage of radar observations over in situ aircraft observations is that the former provide high vertical resolution within the radar sampling volumes. A second advantage is that the radar observations can easily be scaled relative to cloud-top height, while aircraft usually fly level legs at constant heights, and observations along ascents or descents convolve vertical and horizontal variations in the variables sampled (e.g., Gerber et al. 2013). A third advantage is that spectrum width estimates from Doppler radar observations provide a route to TKE dissipation rates (e.g., Fang et al. 2014a, hereafter F14A, 2014b, hereafter F14B). Thus, the advancements provided by cloud radar observations enable quantitative examination of key terms in the TKE budget at cloud top and provide new perspectives on cloud-top entrainment processes.

This case study uses cloud radar (and other) observations made at the U.S. Department of Energy (DOE) Atmospheric Radiation Measurement (ARM) Program's Southern Great Plains (SGP) site (Mather and Voyles 2013). A brief background on entrainment formulation and the different techniques we use to calculate entrainment rates is given in the next section. The data used in this study have been reported extensively in F14A and F14B; we describe it briefly in section 3. Calculations of the variance term and the dissipation rate term in the TKE budget at cloud top from radar observations and budget estimates and parameterizations of entrainment rates are in section 4.

## 2. Background and entrainment formulations

Several methods have been proposed to calculate (estimate) entrainment rates and evaluate and apply entrainment rate parameterizations by using observations or model-derived parameters from simulations. Below, we discuss the TKE budget that provides the basic formulation for currently used entrainment rate parameterizations in stratocumulus clouds. We also include a discussion of how observations and models are used for developing and evaluating entrainment parameterizations.

### a. *TKE budget of the entrainment zone and entrainment parameterizations*

We formulate the cloud-top entrainment rate by applying the steady-state TKE budget at the inversion base. Following Tennekes and Driedonks (1981), this budget may be written as

$$0 = \frac{g}{\theta_0}(\overline{\theta_v' w'})_i - \frac{\partial}{\partial z}(\overline{ew'} + \overline{p'w'}/\rho)_i - (\overline{u'w'}\Delta U/d + \overline{v'w'}\Delta V/d) - \varepsilon_i, \quad (1)$$

where $e$ is the turbulent kinetic energy, $(\overline{\theta_v' w'})_i$ is the buoyancy flux (virtual potential temperature flux) at the

base of the inversion, the combined vertical transport of TKE and pressure perturbation term is $-(\partial/\partial z)(\overline{ew'} + \overline{p'w'}/\rho)$, the mechanical production due to wind shear across the inversion is $-(\overline{u'w'}\Delta U/d + \overline{v'w'}\Delta V/d)$, and $\varepsilon_i$ is the eddy dissipation rate at the base of the inversion. In Eq. (1), $\theta_0$ is a reference potential temperature, $d$ is the thickness of the inversion layer, and all other parameters follow standard meteorological notation. Without shear and using the virtual potential temperature budget of the inversion layer to represent the buoyancy flux by invoking the flux-jump assumption, Eq. (1) becomes

$$\frac{g}{\theta_0} w_e \Delta\theta_v = -\frac{\partial}{\partial z}(\overline{ew'} + \overline{p'w'}/\rho) - \varepsilon_i, \tag{2}$$

where $w_e$ is the entrainment velocity and $\Delta\theta_v$ is the virtual temperature difference across the inversion. The transport and pressure term is often assumed to be proportional to the vertical velocity variance (to the $^3/_2$ power) as

$$-\frac{\partial}{\partial z}(\overline{ew'} + \overline{p'w'}/\rho) \propto \frac{\sigma_w^3}{h}, \tag{3}$$

where $h$ is assumed to be the BL depth (Tennekes 1973). With this assumption, Eq. (2) can be written as

$$\frac{g}{\theta_0} w_e \Delta\theta_v = C_T \frac{\sigma_w^3}{h} - \varepsilon_i, \tag{4}$$

where $C_T$ is a nondimensional coefficient that needs to be determined empirically. We refer to the term involving $\sigma_w$ as the variance term, since $\sigma_w^3 = (\sigma_w^2)^{3/2}$, and $\sigma_w^2$ is the vertical velocity variance.

The role of the dissipation term in the TKE budget was discussed by Lilly (1968) in his application of the budget to the entire BL. Tennekes (1970) neglected the dissipation term $\varepsilon$ in a formulation that considers the TKE budget at the base of the capping inversion to obtain an entrainment rate parameterization for a dry BL. Zeman and Tennekes (1977) indicate, however, that neglecting $\varepsilon$ may not always be valid. They argue that the dissipation rate can be represented as

$$\varepsilon = C_D \frac{\sigma_w^3}{l_i}, \tag{5}$$

where $l_i$ is the length scale associated with dissipation processes at the bottom of the inversion layer. With this formulation of the dissipation rate, Eq. (4) becomes

$$\frac{g}{\theta_0} w_e \Delta\theta_v = C_T \frac{\sigma_w^3}{h} - C_D \frac{\sigma_w^3}{l_i}. \tag{6}$$

One possibility is that $l_i$ is proportional to $h$ (Zeman and Tennekes 1977), in which case Eq. (6) can be written as

$$\frac{g}{\theta_0} w_e \Delta\theta_v = A_\sigma \frac{\sigma_w^3}{h}, \tag{7}$$

where $A_\sigma = C_T - C_D(h/\ell_i)$.

The vertical integral length scale $l_w$ is formulated as $l_w = \sigma_w^3/\varepsilon = \ell_i/C_D$ from the dissipation rate and the variance. It can be related to the $l_i$ in Eq. (5) as $l_i = C_D l_w$, and Eq. (5) can then be written as

$$\varepsilon = \frac{\sigma_w^3}{l_w}, \tag{8}$$

and thus $A_\sigma = C_T - (h/l_w)$.

We focus on the two terms on the right-hand side of Eq. (4) that combine to give the entrainment velocity and define the unscaled variance entrainment velocity $w_\sigma$ and the eddy dissipation velocity $w_\varepsilon$ by using Eq. (4) to give

$$w_\sigma = \frac{\theta_0}{g\Delta\theta_v} \frac{\sigma_w^3}{h} \tag{9}$$

and

$$w_\varepsilon = \frac{\theta_0}{g\Delta\theta_v} \varepsilon. \tag{10}$$

The entrainment rate (velocity) $w_e$ can then be represented as different combinations of $w_\sigma$ and $w_\varepsilon$ with appropriate values of the bulk coefficients. For example, Eq. (4) can be written as $w_e = A_\sigma w_\sigma$.

Observational studies of cloud-top entrainment have been mostly constrained to the use of aircraft observations. A common approach is to estimate $w_e$ from conserved parameter fluxes below the inversion and divide by the jump in this conserved quantity across the inversion. [See Faloona et al. (2005) for a complete discussion]. Since the vertical velocity variance $\sigma_w^2$ can also be estimated from the aircraft turbulence, Eq. (7) can be used to estimate $A_\sigma$, although there can be uncertainties in the $w_e$ estimates from the flux technique. Faloona et al. (2005) used observations of three different scalar quantities to help establish the uncertainties in this method of estimating the entrainment rates. From Eq. (7), the entrainment velocity can also be written as

$$w_e = A_\sigma \frac{\sigma_w}{R_{i\sigma}}. \tag{11}$$

Here, following Deardorff (1980),

$$R_{i\sigma} = \frac{g}{\theta_0}\frac{\Delta\theta_v h}{\sigma_w^2}. \tag{12}$$

Laboratory, observational, and modeling studies have been used to estimate various forms of the $A$ coefficients. Implicit in the application of Eq. (11) is the assumption that the variance terms and dissipation rate terms in the TKE budget are correlated by some constant factor. Another possibility, as discussed by Bretherton and Blossey (2014), is that

$$w_e = A_\varepsilon \frac{\theta_0}{g}\frac{\varepsilon}{\Delta\theta_v}, \tag{13}$$

which follows from Eq. (10). An important feature of this formulation of the entrainment rate is that the depth of the BL is not required for the calculation.

In summary, the formulations described above show that the entrainment velocity near stratocumulus cloud top can be calculated using observations of vertical velocity variance, change in virtual potential temperature across the inversion, and the turbulence dissipation rate along with other standard boundary layer variables.

### b. Entrainment rate parameterization using w*

A common closure assumption is that $\sigma_w = \alpha w^*$, where $w^*$ is the Deardorff velocity (convective velocity scale), and the coefficient $\alpha$ is empirically defined from observations or from LES model simulations. For stratocumulus clouds, $w^*$ is defined as a generalized convective velocity scale, according to Deardorff (1980), as

$$w_*^3 = 2.5(g/\theta_0)\int_0^h \overline{w'\theta_v'}\, dz, \tag{14}$$

where $\overline{w'\theta_v'}$ is the vertical turbulent flux of virtual potential temperature. Equation (7) can be written as

$$w_e = A_{w*}\frac{\theta_0}{g}\frac{w^{*3}}{\Delta\theta_v h}, \tag{15}$$

where $A_{w*} = \alpha^3 A_\sigma = \alpha^3[C_T - C_D(h/\ell_i)]$. Equation (11) can also be written as

$$w_e = A_{w*}\frac{w^*}{R_{iw*}}, \tag{16}$$

where $R_{iw*}$ is the bulk interfacial Richardson number (Deardorff 1980; Nicholls and Turton 1986), defined as

$$R_{iw*} = \frac{g}{\theta_0}\frac{\Delta\theta_v h}{w^{*2}}. \tag{17}$$

Thus, if $A_{w*}$ (or $C_E$) is known, the entrainment rate can be parameterized in terms of the convective velocity scale, the inversion strength, and the depth of the BL. Since for these observations we do not have the vertical profile of the virtual heat flux needed to calculate $w^*$ in Eq. (14), we use the formulation proposed by Lock and MacVean (1999) and Ghate et al. (2014). Using the surface convective velocity scale $w_s^*$ (calculated by using the surface buoyancy flux) and the radiative convective velocity scale $w_r^*$ (based on the radiative flux divergence across the cloud layer), the total convective velocity scale $w_t^*$ is

$$w_t^{*3} = w_s^{*3} + w_r^{*3}. \tag{18}$$

This enables us to calculate the entrainment rate as a function of the turbulence forcing mechanism and the inversion strength. The above technique is similar to that adopted by Lock et al. (2000), although it differs from their formulation in that it does not account for the effects of wind shear and buoyancy reversal, which could be important in some cases (Wang et al. 2008; Mellado et al. 2014). In the case presented here, these effects are small, since the wind speed shear is weak (despite strong directional shear), and the buoyancy reversal is not relevant since the equivalent potential temperature jump is positive (F14A).

The formulation described in this section indicates that the entrainment rate near stratocumulus cloud top can be calculated with prior knowledge of the surface buoyancy flux, cloud-layer radiative flux divergence, and other standard boundary layer variables.

### c. Entrainment rate from boundary layer mass budget

Radar observations alone can be used to calculate $w_\sigma$ and $w_\varepsilon$, but an independent estimate of the entrainment rate is needed to provide the bulk coefficients in Eqs. (11), (13), and (16). Here we use a budget of the BL height to estimate entrainment rates according to the technique outlined by Stevens et al. (2003) and Faloona et al. (2005). From the BL-height budget (derived from mass conservation), the local time variation of the inversion height $z_i$ may be written as

$$\frac{\partial z_i}{\partial t} = -\mathbf{V}_h \cdot \nabla z_i + w_i + w_e, \tag{19}$$

where $w_i$ is the large-scale vertical velocity at the inversion and $w_e$ is the entrainment rate. The horizontal advection of the inversion height is $-\mathbf{V}_h \cdot \nabla z_i$, where $\mathbf{V}_h$ is the horizontal wind vector. Equation (19) can be used to estimate the entrainment rate if the large-scale vertical velocity, the local tendency, and the horizontal advection of $z_i$ are known. Aircraft studies (Stevens

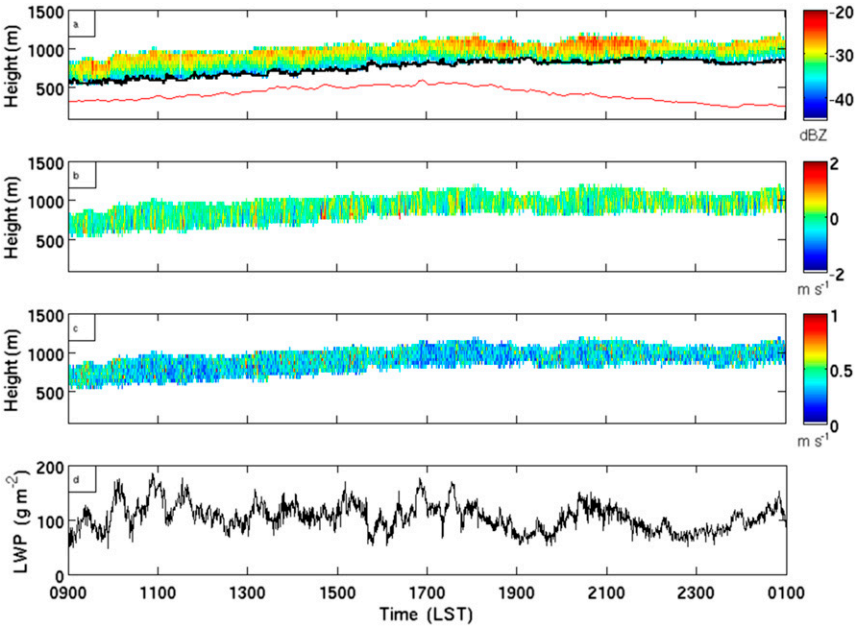


FIG. 1. Time–height display of (a) reflectivity factor, (b) mean Doppler velocity, and (c) Doppler spectrum width recorded by the millimeter-wave cloud radar, and (d) liquid water path from the microwave radiometer. The ceilometer-recorded cloud-base height (black) and the lifting condensation level calculated from surface observations (red) are also shown in (a).

et al. 2003; Faloona et al. 2005) have used a Lagrangian framework so that the total derivative (local and advective term combined) of the inversion height can be estimated. In this study, we estimate both the local and advective terms. As in previous studies, the large-scale vertical velocity at the inversion is estimated by using values from large-scale model analyses.

## 3. Data and case description

The observations used in this work were obtained at the ARM SGP site, which has been in operation since 1992. The observations for the case considered were from a nonprecipitating stratocumulus cloud that persisted over the site from 0930 local standard time (LST) 25 March to 0030 LST 26 March 2005. This case is described in detail in F14A and F14B, and a portion of the case (0930–1230 LST) was modeled by Zhu et al. (2010) and compared with the ARM observations. Radar observations of the cloud, with the ceilometer cloud-base height and lifting condensation level (LCL) calculated from near-surface temperature and moisture, are shown in Fig. 1. The general rise in the depth of the BL and the turbulent characteristics of the cloud are clearly visible. Although the cloud-top height generally increases with time during the first 9 h, the cloud depth does not change appreciably during the entire observing period. Since the LCL is calculated using the near-surface values, it is observed (as expected) systematically below the ceilometer cloud-base height. The difference becomes more exaggerated after sunset when the boundary layer becomes decoupled.

This case was selected for previous studies (F14A, F14B; Zhu et al. 2010) because of the range of turbulence forcing due to variability in the surface buoyancy fluxes and the documented cloud-top radiative cooling. During the day, solar absorption by the cloud minimized cloud-top cooling, particularly around local noon, although sufficient solar radiation was transmitted though the cloud to heat the surface and give rise to surface buoyancy fluxes. During the evening and the night, middle- and upper-level clouds present over the site at various times diminished the cloud-top cooling (F14A).

The observations from the SGP millimeter cloud radar (MMCR; Moran et al. 1998) provide a description of the cloud reflectivity, Doppler velocity, and Doppler spectrum width, according to the MMCR sampling strategy described by Kollias et al. (2007). F14B provides a detailed description of the radar-derived turbulence quantities used in this study.

The total vertical velocity variance $\sigma_w^2$ used here is the sum of the resolved variance (horizontal scales greater than about 30 m) calculated from the radar vertical velocity fluctuations relative to 60-min averages at each height and the subvolume radar sampling variance

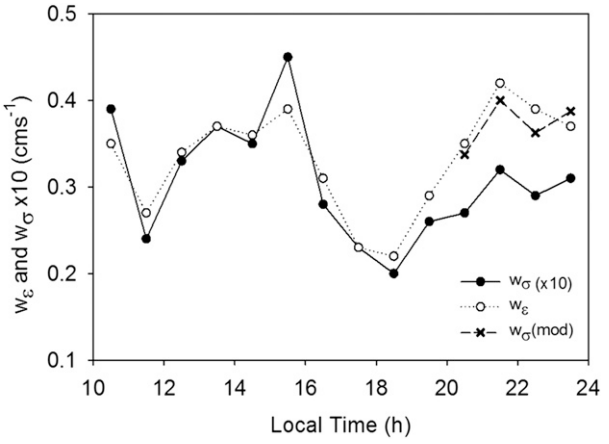


FIG. 2. Entrainment velocity from eddy dissipation rate and from the vertical velocity variance terms in the TKE budget and as given by Eqs. (9) and (10), with modified velocity variance terms obtained for the 2030–2330 LST hourly values for a reduced BL depth due to decoupling.

(scales less than 30 m) from the spectrum width. This total variance provides an estimate of the variance equivalent to that measured from aircraft or towers, where the inertial subrange is resolved; however, the radar variance estimates might not be equivalent to the resolvable-scale variance in LES, where the subgrid variance is parameterized.

The spectrum width observations provide a means to estimate the eddy dissipation rate $\epsilon$ [Eq. (4) of F14B]. This formulation assumes that the turbulence broadening of the Doppler spectrum (as characterized by the spectrum width) is three-dimensional and isotropic and that it falls within the inertial subrange. Although the spectrum width can be calculated at each sampling interval, some averaging is needed to reduce the noise associated with a single estimate to give $\overline{\varepsilon}$. For this case, the hourly averaged dissipation rates calculated at all levels and times within the cloud vary from about $0.6 \times 10^{-3}$ to $1.8 \times 10^{-3}\,\mathrm{m^2\,s^{-3}}$, with an average for the entire period of $1.2 \times 10^{-3}\,\mathrm{m^2\,s^{-3}}$ (F14B).

## 4. Turbulence and entrainment at cloud top

The radar observations can be used to characterize the variance and dissipation terms in the entrainment zone [Eq. (4)], but values of the bulk coefficients are required to convert the unscaled turbulence velocities to entrainment rate estimates. With these coefficients, we can estimate cloud-top entrainment rates from the observations and verify the entrainment rate parameterizations used in models. Here, we use an estimate of the entrainment rate averaged over the period of observations to provide values for the bulk coefficients.

### *a. Cloud-top turbulence velocities from radar observations*

The variance $w_\sigma$ and the dissipation $w_\varepsilon$ velocities calculated from Eqs. (9) and (10) are shown in Fig. 2. For this calculation, the 1-h averages of the cloud-top height are used for the BL depth $h$ ($\overline{h}$ = 1040 m); the average inversion strength $\Delta\theta_v$ is 12° ± 1°C, as estimated from the soundings made on this day (F14A), and $\theta_0$ is 282 K. The variance velocity has a magnitude of about 10% of the dissipation velocity (i.e., $\overline{w_\sigma} \approx 0.09\overline{w_\varepsilon}$, where the overbar indicates the average), and the two velocities are highly correlated. This correlation, however, occurs partly because the total $w$ variance used for calculation of the variance velocity is the sum of the directly resolved radar variance and that associated with the radar spectrum width, which is also used to estimate the dissipation rate. Although the correlation is high, $w_\varepsilon$ is about 25% greater than $11w_\sigma$ after 2000 LST. Although the cloud-top radiative cooling is stronger and the surface forcing is weaker at night, these differences do not appear to play a major role in explaining differences in magnitude of the variance and dissipation velocities. These daytime values of these quantities do not show major differences despite the strong variability in the cloud top and the surface forcing during the day (F14A). There is, however, evidence that the BL becomes decoupled later in the night. A sounding made at 2400 LST (see Fig. 2 in F14A) indicates a temperature increase of about 1°C and a mixing ratio decrease of about $0.5\,\mathrm{g\,kg^{-1}}$ at a height of about 200 m, which is indicative of decoupling. Thus, the BL depth $h$ in Eq. (9) should be reduced by 200 m near the end of the period, which would increase $w_\sigma$ by about 20%. The onset time of the decoupling is uncertain; however, if the variance velocities from 1830 to 2330 LST are increased by 20%, the nighttime values are in much better agreement with the dissipation rate velocities, as shown in Fig. 2. The correlation between $w_\sigma$ and $w_\varepsilon$ increases from 0.78 to 0.94 when $h$ in Eq. (9) is reduced for the last 4 h of observation. With this adjustment $\overline{w_\varepsilon} \approx 10\overline{w_\sigma}$.

A further display of the ratio $w_\sigma/w_\varepsilon$ as a function of the ratio of the vertical scale length $l_w$ to the BL depth $h$ ($l_w/h$) is in Fig. 3. A strong correlation between these two ratios is expected, because the vertical scale length is a function of variance and dissipation rate. However, the lower ratios are clearly prevalent at night when turbulence is estimated using the cloud-top height for $h$ in Eq. (9). Nevertheless, increased ratios are associated with a decrease in $h$ due to decoupling at night (see Fig. 2), and we see a tighter clustering of points around a ratio of

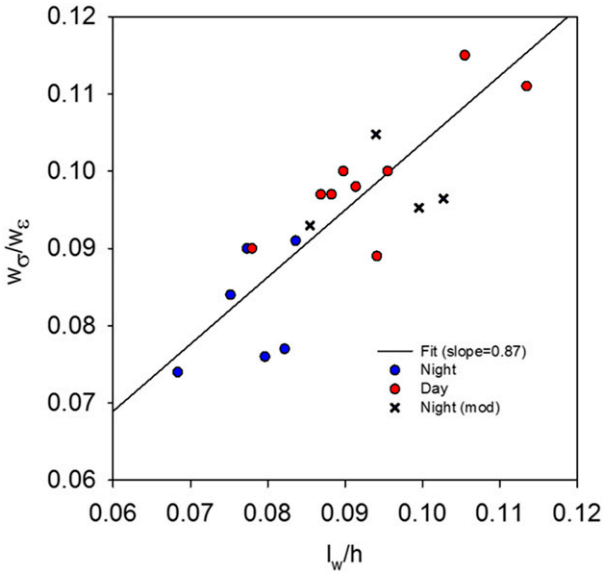


FIG. 3. Ratio of $w_\sigma$ to $w_\varepsilon$ as a function of the ratio of $l_w$ to $h$, with a linear fit to the hourly observations and modified ratios for 2030–2330 LST (×) for a reduced BL depth due to decoupling.

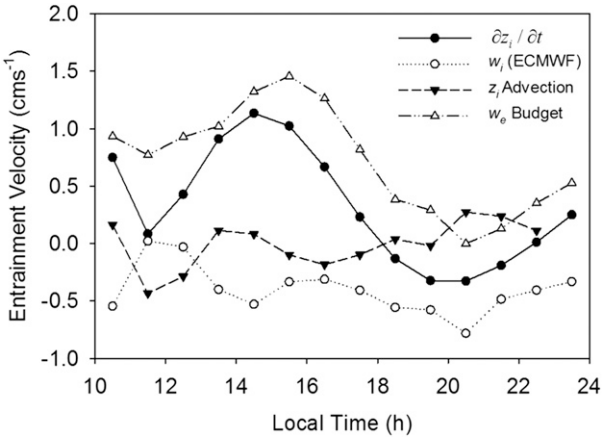


FIG. 4. Entrainment velocity from the inversion budget and the local $h$ time derivative, advection, and large-scale vertical velocity terms in the budget. For the advection and vertical velocity terms, the dashed and dotted lines represent cubic fits to the hourly values.

about 0.09. Because the ratio has a small variance, these observations validate the assumption that the energy dissipation rate term to the first order is related to the large-scale variance term by a nearly constant ratio of two height scales such that, on average, $w_\sigma/w_\varepsilon \approx l_w/h \approx 0.1$. However, this constant ratio is confirmed only for this case, and day–night differences might be important. The nighttime values have vertical scale lengths (F14B) of about 85 m, while the daytime values are about 95 m. Thus, some differences in the character of the large eddies and the turbulence forced might result when surface buoyancy generation is added to the cloud-top cooling. The reduced vertical length scales at night also occur as the BL becomes decoupled and $h$ is less than the cloud-top height.

### b. *Entrainment from inversion-height budget*

The terms in the inversion-height budget in Eq. (19) are estimated by using observations from the SGP site and large-scale model analyses. The observed local variation of the inversion height from the radar-determined cloud-top height over 15 h of observation gives the local time variation of the inversion height. Since this term in Eq. (19) is the derivative, we fit the 15 h of inversion heights to a seventh-order polynomial to remove shorter-time-scale variations that can amplify the derivative. See the appendix for a comparison of the hourly average height and the polynomial fit. The time derivative of the seventh-order polynomial gives hourly values of $\partial z_i/\partial t$, as shown in Fig. 4 for the 13-h period from 1030 to 2330 LST with 1 h of observations at the beginning and the end of the 15-h period removed. This truncated series is used for the budget terms since the cloud-top height exhibits a sharp jump of about 100 m at 0930 LST (see Fig. 1) and the horizontal advection term (discussed below) shows large fluctuations after 2330 LST. The local derivative is positive during the day, with a maximum of about 1 cm s$^{-1}$ at about 1430 LST. From 1800 to 2300 LST, the derivative is slightly negative. The average cloud-top velocity for the period 1030–2330 LST is 0.32 cm s$^{-1}$ (Table 1), with an uncertainty of about ±0.05 cm s$^{-1}$ (see the appendix).

A direct determination of the advection term is difficult, because neither an array of cloud radars nor a scanning radar was operated at the SGP site to enable horizontal mapping of the cloud-top height and winds. However, a triangular array (with sides of about 250 km) of ceilometers and microwave radiometers at ARM SGP boundary facilities (B1, B4, and B5) is centered on the central facility site (C1; appendix). These instruments provide estimates of cloud-base height $z_b$, cloud liquid water path (LWP), and BL winds. By assuming that the cloud water content is adiabatic, the cloud-top height can be estimated from the LWP and the cloud-base height (Albrecht et al. 1990). The cloud-top-height retrieval method and applications to the three boundary sites and the central site are described in

TABLE 1. Values of terms in Eq. (19) (cm s$^{-1}$), averaged from 1030 to 2230 LST.

| $\partial z_i/\partial t$ | $-\mathbf{V}_h \cdot \nabla z_i$ | $w_i$ | $w_e$ |
|---|---|---|---|
| 0.32 | −0.01 | −0.41 | 0.74 |

the appendix. Since the winds near the inversion height have a direction of north-northwest (about 300°) (F14A), we use the retrieved cloud-top heights from sites north and southeast (B1 and B5) of the central facility to estimate the inversion advection term for wind speeds from the wind profiler located at the central facility (F14A). The hourly values of the advection term are shown in Fig. 4. The amplitude of the advection term is less than that of the local derivative, and this term is out of phase with the time derivative of the BL height. The advection term for the period is close to zero ($-0.01\,\mathrm{cm\,s^{-1}}$), with an estimated uncertainty of $\pm 0.1\,\mathrm{cm\,s^{-1}}$ (see the appendix), although our confidence in the time evolution of this term is substantially less than for the local derivative term.

The 900-hPa vertical velocities (based on omega) from the European Centre for Medium-Range Weather Forecasts (ECMWF) reanalysis are used to estimate $w_i$. There is relatively little temporal variation in the vertical velocity from the reanalysis (Fig. 4). The average for the 13-h period of $-0.41\,\mathrm{cm\,s^{-1}}$ is similar to the average of vertical velocities from a constrained variational analysis approach (Zhang and Lin 1997; Zhang et al. 2001) of $-0.49\,\mathrm{cm\,s^{-1}}$. However, the variational $w_i$ varies substantially during the period ($\pm 2\,\mathrm{cm\,s^{-1}}$), compared with the vertical velocity estimates from the ECMWF ($\pm 0.2\,\mathrm{cm\,s^{-1}}$). The ECMWF estimates are used here, with an estimated error in the average of about $\pm 0.1\,\mathrm{cm\,s^{-1}}$. But we do recognize that the temporal variations in the ECMWF values are also uncertain.

The 13-h averages of the terms in Eq. (19) are shown in Table 1, along with $w_e$ estimated as the residual. On average, the inversion height increases during this period at a rate similar in magnitude to the vertical velocity subsidence rate. The averaged horizontal advection term is close to zero, with some variation during the day. Also, as explained in the appendix, the average was obtained without the hours at the beginning and the end of the time series, because the advection term was nearly constant during the entire period except for a large positive fluctuation at the end of the observing period. If these larger values are included, the average advection term is $-0.06\,\mathrm{cm\,s^{-1}}$. With the averages shown in Table 1, the entrainment rate is estimated to be $0.74\,\mathrm{cm\,s^{-1}}$. This estimate is on the high end of estimates ($0.1$–$0.8\,\mathrm{cm\,s^{-1}}$) made in previous studies of marine stratocumulus clouds (Nicholls and Turton 1986; Kawa and Pearson 1989; Faloona et al. 2005).

In the inversion-height calculation used here, the uncertainty in the entrainment estimate is due to uncertainty in the vertical velocity estimate and the horizontal advection. Uncertainties of about $0.1\,\mathrm{cm\,s^{-1}}$ for these two terms would give a root-mean-square (RMS) uncertainty of $\pm 0.15\,\mathrm{cm\,s^{-1}}$, so the average entrainment rate from the inversion-height budget is estimated at $0.74 \pm 0.15\,\mathrm{cm\,s^{-1}}$ for this case, with about 20% uncertainty.

All of the terms in Eq. (19) have temporal variability (Fig. 4), though only the $\partial z_i/\partial t$ term is obtained with confidence for any 2-h interval in the sampling period. The seventh-order polynomial fit ensures a smooth variation of the local derivative of the cloud-top height (BL height), with a maximum at 1430 LST and a minimum at 2000 LST. The increase in the time derivative during the afternoon is associated with the maximum surface heating at this time and a decrease in solar absorption at cloud top that compensates for longwave cooling near local noon as described in F14B. During the evening, the decreases in surface buoyancy fluxes and in cloud-top radiative cooling are due to the presence of midlevel clouds above the stratus that suppress longwave cooling and result in a decrease in the inversion height because of weakened entrainment. The vertical velocity from the ECMWF analyses and the advective estimates show much smaller temporal variations than the inversion-height derivative. Consequently, the entrainment rate variations from the budget estimated by Eq. (19) mostly reflect variations in the local time derivative of the inversion height, with a midafternoon maximum of about $2\,\mathrm{cm\,s^{-1}}$ and a minimum close to zero at 2100–2200 LST. Although local variations in the cloud-top height can be resolved with confidence, the temporal uncertainty in the vertical velocity and the advection terms is large and reflects the difficulty in making these measurements with the observations available for this study.

### c. *Entrainment rates from parameterizations*

The average entrainment rate of $0.74\,\mathrm{cm\,s^{-1}}$ (Table 1) is used to evaluate the bulk coefficients introduced into the formulations from the TKE budget presented above. Using this value in Eqs. (4) and (7) with the observed turbulence terms gives $C_T = 37$ and $A_\sigma = 26$. If we use the nighttime values corrected for decoupling, as discussed above, then the coefficients become $C_T = 33$ and $A_\sigma = 23$; however, the uncertainty in the average entrainment rate from the TKE budget (about 20%) results in similar total uncertainty in the estimates of these coefficients. Further, because the inversion strength is assumed to be constant in this case, these coefficients must be considered valid for a limited range of inversion stabilities. In this case $A_\sigma$ is more than double the Nicholls and Turton (1986) value of 10. However, their $R_{i\sigma}$ is 500, while the average $R_{i\sigma}$ in this study is about 1700 with a similar $\sigma_w$ of about $0.5\,\mathrm{cm\,s^{-1}}$. Thus, the

smaller $R_{i\sigma}$ in Nicholls and Turton (1986) is due to the weaker inversion and lower BL depth. Further, the average entrainment rate of Nicholls and Turton (1986) is about 0.50 cm s$^{-1}$, roughly two-thirds of the value in this study. These two effects give a higher $A_\sigma$ in this study than in Nicholls and Turton (1986). If both the variance and the dissipation rate terms are known, Eq. (4) can give the entrainment rate by using $C_T$. If we assume the dissipation rate to be proportional to the variance with the scaling shown in Eq. (5), then the entrainment rate can be estimated by using Eq. (11), which is one of the most common assumptions used in parameterizations and is implicit in the $w^*$ scaling given by Eq. (16).

For the case here, the mean $w_e$ for the period used in Eq. (13) would give $A_\varepsilon = 2.3$. In Bretherton and Blossey (2014), LES model results give an $A_\varepsilon \approx 3$ that is nearly constant in their simulations, despite strong diurnal variation in the LES entrainment rates. Although the $A_\sigma$ and $A_\varepsilon$ closure coefficients can be used in entrainment parameterizations in models of varying complexities, they can also be used to estimate entrainment rates from radar observations of the variance and the dissipation rate terms.

We use the hourly $w_t^*$ [Eq. (18)] values for this case (from F14A) to calculate the mean $\overline{w_t^*}$ for the entire time period as $1 \pm 0.3$ m s$^{-1}$. If we use this value in Eq. (15), the coefficient $A_{w*}$ has a value of about 3, and $R_{iw*}$ is 420. This value of $A_{w*}$ (and $R_{iw*}$) is larger than the $A_{w*}$ value of approximately 2 [Table 1 of Nicholls and Turton (1986)] and $A_{w*} \approx 1$ for average values given by Faloona et al. (2005). We recognize, however, the uncertainties in both the $w^*$ and $w_e$ estimates from our study. Because the entrainment rate is proportional to $w_t^*$ to the third power, these uncertainties can lead to large uncertainties in $A_{w*}$. For example, if we calculate $w_t^*$ as a simple sum of $w_s^*$ and $w_r^*$ ($w_{ts}^*$), the average scaling velocity is $1.3 \pm 0.5$ m s$^{-1}$, $A_{w*}$ will be 1.4, and $R_{iw*}$ will be 260—values closer to the values of Nicholls and Turton (1986) and Faloona et al. (2005). These calculations also point out the sensitivity of $A_{w*}$ estimates as a result of relatively small variations in $w^*$, again because of the cubic relationship of $w^*$ to the entrainment rate. A 20% bias error in $w^*$ will result in a 60% uncertainty in the total error uncertainty in $A_{w*}$. Thus, for a 20% bias in $w_e$, $h$, $\Delta\theta_v$, and $w^*$, the total error in the $A_{w*}$ estimate will be 120%. If the errors (uncertainties) are random, the probable (RMS) error would be 50% if each of the four terms had a 20% random error.

### d. *Entrainment rate comparisons from different techniques*

One advantage of radar retrievals of entrainment rates over standard aircraft techniques is that estimates can be made with observations averaged over 1 h or less. Because of the close relationship between the variance term and the dissipation terms in this case, the entrainment rate can be estimated directly by using various combinations of these terms. Thus, for these surface-based radar measurements, the temporal evolution of entrainment rates can be obtained if the transfer coefficients are known. The hourly values of the entrainment rates obtained from Eq. (4) with $C_T = 37$ are shown in Fig. 5. This estimate includes both variance and dissipation rate terms but does not include a BL depth correction for nighttime decoupling. The entrainment rates for only the hourly averaged dissipation values are also shown in Fig. 5 for $A_\varepsilon = 2.3$. These two estimates mirror the unscaled velocity results shown in Fig. 2 and show the highest rates during the hours when both surface fluxes and radiative fluxes are operating. If the decoupling adjustment is made, the minimum occurs in the evening after the surface forcing ceases and an upper-level cloud deck diminishes the cloud-top cooling.

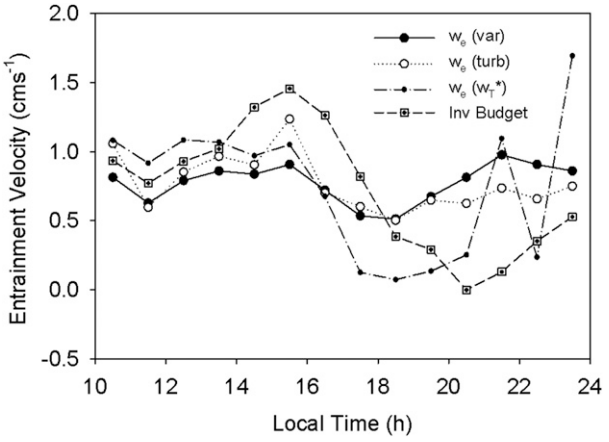


FIG. 5. Entrainment velocities as a function of time from the turbulence term [variance and dissipation from Eq. (4) with $C_T = 37$], the dissipation term [from Eq. (13) with $A_\varepsilon = 2.3$], and the convective velocity scale (cubic sum) parameterization, with entrainment velocity from the height budget for smoothed advection and vertical velocity.

The parameterized entrainment rates estimated by using $w_t^{*3}$ follow the entrainment rate estimated from the turbulence terms, but they have a larger amplitude variation and a minimum close to zero in the evening hours. Estimates of the time variations in entrainment rates from the inversion budget [Eq. (19)] in Fig. 5 also have a much larger range than the turbulence estimates, although (as discussed previously) there is substantial uncertainty in the amplitude of this variation. Nevertheless, all estimates show values in the morning that decrease to a relative minimum around noon and then increase to a maximum later in the day. The budget

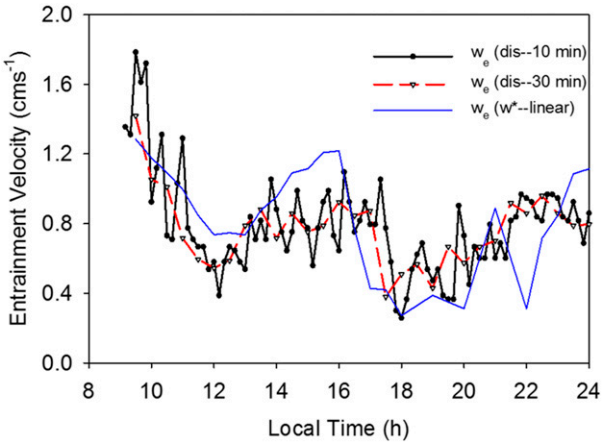


FIG. 6. Entrainment rates estimated from radar-derived dissipation rates for 10- (black) and 30-min (red) averages and from the convective velocity scale (linear average; blue), with parameterization coefficients giving an average entrainment velocity for the 13-h time period of 0.76 cm s$^{-1}$.

estimates have a minimum around 2000–2200 LST compared with a minimum at around 1800 LST for the other terms. The amplitude of the variations from the radar turbulence terms is about half the amplitude of the inversion budget and the convective velocity–scale estimates.

One advantage of estimating the entrainment rate from the spectrum width (dissipation term) is that the entrainment rate can be estimated at a substantially higher rate than in the case of variance term estimates, which require making averages over periods of 30–60 min. Further, no scale length is needed in the estimates made by using Eq. (13), which eliminates the difficulty in defining these length scales when the BL becomes decoupled. To illustrate the capability to obtain high-temporal-resolution entrainment rates, the time variations of the 10- and 30-min entrainment rate means (from the dissipation rate term only) are shown in Fig. 6. The high-temporal-resolution entrainment rates for this case indicate variability on a time scale of about 40–50 min (about five cycles over a 3.5-h period around 1500 LST in Fig. 6), which for an advection velocity of 5 m s$^{-1}$ corresponds to variability on scales of 12–15 km (mesoscale). These variations are on a scale that is similar to the mesoscale variability in the liquid water path shown in Fig. 1. The mesoscale variability illustrates why estimates from the variance require longer averaging or appropriate filtering of the vertical velocity to ensure that mesoscale variability is removed from the variance estimates. In the results shown in Fig. 6, entrainment rates calculated from a scaling of the simple combined convective velocity (30-min) scale are compared with the rates calculated from the dissipation rate estimates for 10- and 30-min averages. Correspondence between these two parameterized entrainment rates is good on scales of 1–2 h. The simple linear relationship of $w^*$ to entrainment captures the daytime variability more effectively than does the calculation based on the cubic relationship that is more commonly used in parameterizations based on Eq. (15). Faloona et al. (2005) also found a best fit of their $w_e$ values as a function of $1/\sqrt{R_{iw^*}}$, which is proportional to a linear function of $w^*$.

## 5. Discussion and conclusions

Observations from a zenith-pointing Doppler cloud radar are used to examine the vertical velocity variance and energy dissipation rate at the top of continental stratocumulus clouds. The observations were made in a continental stratocumulus cloud over the DOE ARM SGP site for a 15-h period. Clouds were uniform during this entire period, with thicknesses of 300–400 m and tops increasing on average to 800–1200 m. The turbulence forcing due to surface buoyancy fluxes and radiative cooling at cloud top is obtained from surface flux measurements and radiative transfer calculations based on cloud characteristics derived from Doppler cloud radar and lidar observations (F14A, F14B). Vertical velocity and spectrum width observations from the upward-pointing MMCR at the SGP site provide the turbulence in the top 20% (60–80 m) of the cloud, which is defined as the entrainment zone. The spectrum width directly yields energy dissipation rates in the entrainment zone, and the vertical velocity observations provide vertical velocity variance for 1-h periods. These quantities are used to examine the terms in the TKE budget in this layer.

For the 15 h of observations used in this study, the variance term is strongly correlated to the dissipation rates in the entrainment zone. However, the ratio of the variance term to the dissipation rate term is about 20% higher during the day than at night. An observed decoupling of the BL at night results in a 20% reduction in the BL depth $h$. If a reduced $h$ value is used for the variance term estimates, agreement with the variance and dissipation estimates is excellent. Further, at night the vertical length scale $\ell_i$ is reduced such that the ratio $\ell_i/h \approx 0.1$ is relatively constant if a reduced $h$ is used for the nighttime values.

An estimate of the entrainment rate for a 13-h average of the terms in an inversion budget provides an estimate of the average entrainment rate of $0.74 \pm 0.15$ cm s$^{-1}$. This entrainment rate provides estimates for closure coefficients in commonly used parameterizations, which have been evaluated previously by using aircraft observations and models. The coefficients in this study

differ from those estimated previously, but the differences may be due to uncertainties in the parameters used to estimate the coefficients. Errors in the estimates of $A_{w*}$, for example, can be as large as 100%. The coefficients from the inversion budget average entrainment rate are used to develop entertainment rate estimates at 1-h intervals for the entire observing period. These rates compare reasonably well with the convective velocity scales $w_t^*$ calculated from the surface buoyancy fluxes and cloud-top radiative cooling and show a similar diurnal pattern.

This case study provides a unique estimate of cloud-top entrainment rates and processes at temporal resolutions that are not practical with other observing systems. In this case, a range of forcing due to variations in the surface buoyancy fluxes and cloud-top radiative cooling contribute to variability in the cloud-top entrainment rates and processes. Further, the use of estimates of the eddy dissipation rate provides a means to advance our capability to estimate entrainment rates remotely and by using dissipation rates observed from other platforms (e.g., airborne cloud radar).

Using the eddy dissipation rate to determine entrainment rates has two major advantages. First, unlike estimates from the vertical velocity variance, no height scale or mixing-length scales are needed, as noted by Bretherton and Blossey (2014). Second, statistically stable representations of the entrainment velocity can be made to allow for retrievals at higher temporal resolution than possible from the vertical velocity variance estimates. Thus, unlike in situ measurements from aircraft, the assumption of stationary and homogeneity on larger scales can be relaxed. It is also difficult to characterize turbulence structures in the entrainment zone from an aircraft when undulating cloud tops are present, because both constant-height flight levels and pseudosoundings make it difficult to define measurements in layers relative to the cloud top. Instantaneous radar observations can be made at a constant distance from the cloud top or at a nondimensional height scaled by the cloud depth. Thus, even with variations in the cloud-top height, radar observations can be made for different formulations of the entrainment zone.

The methods described here, however, have some shortcomings. The entrainment rate estimates needed for radar-derived estimates are limited in this case to the accuracy of the entrainment rates from the inversion-height budget only. Improved techniques for making more accurate estimates in the terms of the inversion-height budget would reduce uncertainty in the parameterization coefficients. Using this technique in cases where additional entrainment rate estimates from other techniques are available (e.g., the scalar flux technique) would also reduce the uncertainty in the parameterization coefficients derived from the observations. LES studies applied to these cases could also assist with estimates of these coefficients. The formulations evaluated here are for a single case. Thus, the closure coefficients derived are not sufficiently accurate to be used in any practical application. Although $w_t^*$ does vary in this case, the inversion strength and the BL depth are relatively constant. Estimates from a wider range of inversion stability and BL depth conditions are needed to provide more confidence in the closure coefficients. The entrainment rate estimates from this study were made in nonprecipitating clouds. For precipitating clouds, the broadening of the Doppler spectrum due to the spread of the droplet sizes (terminal velocities) would be a major contributor to the spectrum width, although techniques that separate the contributions of the cloud droplets and the precipitation droplets in the Doppler spectrum might allow for an estimate of the variance and the dissipation rates.

*Acknowledgments.* The authors wish to thank Karen Haugen for helping in manuscript preparation. Bruce Albrecht and Ming Fang were supported by the Office of Science's Biological and Environmental Research (BER) program of the U.S. Department of Energy under the Atmospheric System Research Grant DE-SC-0008599 and the National Science Foundation Grant 1445832. Virendra Ghate was supported primarily by the U.S. Department of Energy's Atmospheric System Research, an Office of Science, Office of Biological and Environmental Research program, under Contract DE-AC02-06CH11357 awarded to the Argonne National Laboratory. Some of the data used in this study were obtained from the Atmospheric Radiation Measurement (ARM) Program sponsored by the U.S. Department of Energy, Office of Science, Office of Biological and Environmental Research, Climate and Environmental Sciences Division. Acknowledgment is made of the use of products from ECMWF's WCRP Level III-A Global Atmospheric Data Archive.

## APPENDIX

### Radar-Derived Cloud-Top Variations and Inversion Advection Estimates for Inversion Budgets

Inversion heights from 1-h averages of radar cloud-top estimates are shown in Fig. A1. Because the inversion-height (here defined by the cloud top) budget given by Eq. (19) requires the time derivative of this height, we fit a seventh-order polynomial to the time variation of height to provide a smooth function of this derivative as a function of time. The fit shown in Fig. A1

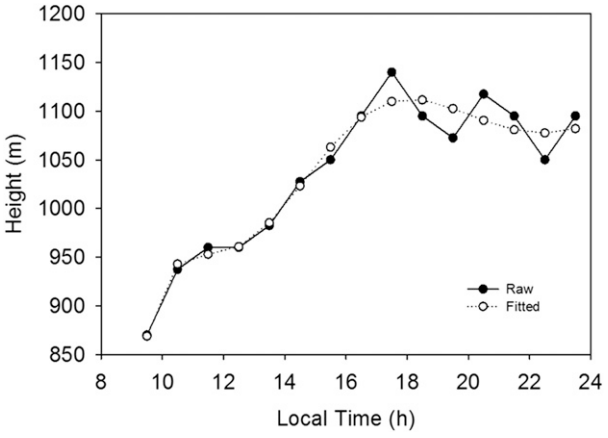


FIG. A1. Cloud-top heights from 1-h average values and a seventh-order polynomial fit.

evens out the short-time-scale fluctuations in inversion height observed during nighttime hours. Although the hourly variability during this period is real and appears to be associated with variations in cloud-top cooling, these oscillations would result in large short-term fluctuations in the time derivative. The uncertainty in the local cloud-top height obtained from the radar for a single profile is ±30 m. Since a 1-h average is based on 900 realizations (F14A), we estimated the standard error to be ±1 m. The time derivative error for a 1-h period is estimated to be ±2 m/3600 s = ±0.06 cm s$^{-1}$. For a 13-h averaging period, this error would be further reduced to about 0.02 cm s$^{-1}$.

The advection term needed for the inversion budget requires an estimate of the horizontal variability of the inversion height, coupled with wind speed and direction. Because the winds were from the north during the entire observing period, we use estimates of the north–south gradient of the inversion height based on observations at three ARM SGP boundary facilities (B1, B4, and B5) around the central facility (C1). The boundary facilities (at locations in Table A1) form a triangle around C1, with B1 about 150 km due north and B4 and B5 about 150 km southeast and southwest, respectively, of C1. Ceilometer cloud-base heights and microwave-radiometer-integrated liquid water path were used, with the assumption that the clouds are adiabatic, to provide estimates of the cloud-top height. This approach follows that of Albrecht et al. [1990; Eq. (4)], so the cloud-top height can be written as

$$z_T = z_b + \left(\frac{2\rho_\ell \mathrm{LWP}}{\rho\Gamma_\ell}\right)^{1/2}, \qquad \text{(A1)}$$

where $\rho$ is the average air density in the cloud layer, $\rho_\ell$ is the density of water, and $\Gamma_\ell$ is the cloud liquid water adiabatic slope (average for the cloud layer). Because the cloud deck in this study is relatively shallow, the assumption of a constant linear increase in the adiabatic liquid water content (constant $\Gamma_\ell$) is reasonable. The adiabatic assumption might result in an overestimate of the inversion height, but this should not affect the spatial derivatives needed to estimate the advection term.

TABLE A1. Location of boundary facilities and central facility at the ARM SGP site.

| Site | Location | Coordinates | Altitude (m) |
|---|---|---|---|
| B1 | Hillsboro, KA | 38.30°N, 97.30°W | 447 |
| B4 | Vici, OK | 36.07°N, 99.24°W | 622 |
| B5 | Morris, OK | 35.69°N, 95.86°W | 217 |
| C1 | Lamont, OK | 36.72°N, 97.48°W | 315 |

The heights retrieved from B1, B4, B5, and C1 by using Eq. (A1) are shown in Fig. A2. General increases in retrieved inversion heights are prevalent at all of the sites during the observing period, although temporal variations are apparent at all of the sites. The inversion heights retrieved from the ceilometer and radiometer at C1 are compared in Fig. A2 with the cloud-top heights from the MMCR cloud-top estimates. Correlation between these two estimates is good, and the retrieved heights (assuming adiabatic cloud) are systematically higher than the values from radar cloud-top heights, as expected. Thus, we have some confidence that the relative changes and the horizontal variations in the heights derived from the three boundary facilities are reasonably captured for the domain defined by the boundary facility sites.

To estimate the $-\mathbf{V}_h \cdot \nabla z_i$ term, we use the winds from the central facility and estimate the gradients by using the B1, B4, and B5 height estimates. We simplify this estimate, because the winds are from the north-northwest

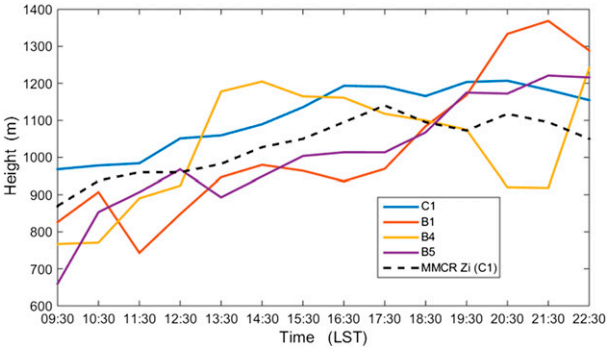


FIG. A2. Inversion-height estimates for the adiabatic assumption with microwave radiometer liquid water path and ceilometer $z_b$ estimated for the SGP central facility C1 and boundary facilities B1, B4, and B5, with direct estimates of the inversion height from the millimeter cloud radar cloud-top measurements.

during the duration of the observations. Thus, we estimate the gradient along the wind by using the horizontal difference between the estimated cloud-top height at B1 and the height at B5 (distance between B1 and B5 is about 320 km and direction from B1 to B5 in wind coordinates is about 330°). We use the median hourly wind speeds at 1 km from the C1 wind profiler (wind speeds varying from 4 to 8 $m\,s^{-1}$; see F14A) in the advection term. The advection term is shown in Fig. 4 as a function of time (F14A). The average advection term for the period is $-0.01\ cm^{-1}$, and the standard deviation is $\pm 0.36\ cm^{-1}$. If we use the horizontal difference between the height at B1 and the average of that at B4 and B5 to calculate the advection using the same winds, the average is $-0.03\ cm^{-1}$. Although our confidence in the temporal evolution of the advection term is low, we estimate the error in the time average to be about $\pm 0.1\ cm\,s^{-1}$. If we consider the standard deviation of the estimate to be due to random errors, the standard error would be $\pm 0.1\ cm\,s^{-1}$.

## REFERENCES


Albrecht, B. A., C. W. Fairall, D. W. Thomson, A. B. White, J. B. Snider, and W. H. Schubert, 1990: Surface-based remote sensing of the observed and the adiabatic liquid water content of stratocumulus clouds. *Geophys. Res. Lett.*, **17**, 89–92, doi:10.1029/GL017i001p00089.

Bony, S., and J.-L. Dufresne, 2005: Marine boundary layer clouds at the heart of tropical cloud feedback uncertainties in climate models. *Geophys. Res. Lett.*, **32**, L20806, doi:10.1029/2005GL023851.

Bretherton, C. S., and P. N. Blossey, 2014: Low cloud reduction in a greenhouse-warmed climate: Results from Lagrangian LES of a subtropical marine cloudiness transition. *J. Adv. Model. Earth Syst.*, **6**, 91–114, doi:10.1002/2013MS000250.

——, and Coauthors, 1999: An intercomparison of radiatively driven entrainment and turbulence in a smoke cloud, as simulated by different numerical models. *Quart. J. Roy. Meteor. Soc.*, **125**, 391–423, doi:10.1002/qj.49712555402.

Brost, R. A., J. C. Wyngaard, and D. H. Lenschow, 1982: Marine stratocumulus layers. Part II: Turbulence budgets. *J. Atmos. Sci.*, **39**, 818–836, doi:10.1175/1520-0469(1982)039<0818:MSLPIT>2.0.CO;2.

Deardorff, J. W., 1980: Stratocumulus-capped mixed layers derived from a three-dimensional model. *Bound.-Layer Meteor.*, **18**, 495–527, doi:10.1007/BF00119502.

Faloona, I., and Coauthors, 2005: Observations of entrainment in eastern Pacific marine stratocumulus using three conserved scalars. *J. Atmos. Sci.*, **62**, 3268–3285, doi:10.1175/JAS3541.1.

Fang, M., B. A. Albrecht, V. P. Ghate, and P. Kollias, 2014a: Turbulence in continental stratocumulus, part I: External forcings and turbulence structures. *Bound.-Layer Meteor.*, **150**, 341–360, doi:10.1007/s10546-013-9873-3.

——, ——, ——, and ——, 2014b: Turbulence in continental stratocumulus, part II: Eddy dissipation rates and large-eddy coherent structures. *Bound.-Layer Meteor.*, **150**, 361–380, doi:10.1007/s10546-013-9872-4.

Frisch, A. S., D. H. Lenschow, C. W. Fairall, W. H. Schubert, and J. S. Gibson, 1995: Doppler radar measurements of turbulence in marine stratiform cloud during ASTEX. *J. Atmos. Sci.*, **52**, 2800–2808, doi:10.1175/1520-0469(1995)052<2800:DRMOTI>2.0.CO;2.

Gerber, H., G. Frick, S. P. Malinowski, H. Jonsson, D. Khelif, and S. K. Krueger, 2013: Entrainment rates and microphysics in POST stratocumulus. *J. Geophys. Res. Atmos.*, **118**, 12 094–12 109, doi:10.1002/jgrd.50878.

Ghate, V. P., B. A. Albrecht, and P. Kollias, 2010: Vertical velocity structure of nonprecipitating continental boundary layer stratocumulus clouds. *J. Geophys. Res.*, **115**, D13204, doi:10.1029/2009JD013091.

——, ——, M. A. Miller, A. Brewer, and C. W. Fairall, 2014: Turbulence and radiation in stratocumulus-topped marine boundary layers: A case study from VOCALS-REx. *J. Appl. Meteor. Climatol.*, **53**, 117–135, doi:10.1175/JAMC-D-12-0225.1.

Haman, K. E., S. P. Malinowski, M. J. Kurowski, H. Gerber, and J. L. Brenguier, 2007: Small scale mixing processes at the top of a marine stratocumulus—A case study. *Quart. J. Roy. Meteor. Soc.*, **133**, 213–226, doi:10.1002/qj.5.

Kawa, S. R., and R. Pearson Jr., 1989: An observational study of stratocumulus entrainment and thermodynamics. *J. Atmos. Sci.*, **46**, 2649–2661, doi:10.1175/1520-0469(1989)046<2649:AOSOSE>2.0.CO;2.

Kollias, P., and B. Albrecht, 2000: The turbulence structure in a continental stratocumulus cloud from millimeter-wavelength radar observations. *J. Atmos. Sci.*, **57**, 2417–2434, doi:10.1175/1520-0469(2000)057<2417:TTSIAC>2.0.CO;2.

——, M. A. Miller, E. P. Luke, K. L. Johnson, E. E. Clothiaux, K. P. Moran, K. B. Widener, and B. A. Albrecht, 2007: The Atmospheric Radiation Measurement Program cloud profiling radars: Second-generation sampling strategies, processing, and cloud data products. *J. Atmos. Oceanic Technol.*, **24**, 1199–1214, doi:10.1175/JTECH2033.1.

Kurowski, M. J., S. P. Malinowski, and W. Grabowski, 2009: A numerical investigation of entrainment and transport within a stratocumulus-topped boundary layer. *Quart. J. Roy. Meteor. Soc.*, **135**, 77–92, doi:10.1002/qj.354.

Lilly, D. K., 1968: Models of cloud-topped mixed layers under a strong inversion. *Quart. J. Roy. Meteor. Soc.*, **94**, 292–309, doi:10.1002/qj.49709440106.

Lock, A. P., and M. K. MacVean, 1999: The parameterization of entrainment driven by surface heating and cloud-top cooling. *Quart. J. Roy. Meteor. Soc.*, **125**, 271–299, doi:10.1002/qj.49712555315.

——, A. R. Brown, M. R. Bush, G. M. Martin, and R. N. B. Smith, 2000: A new boundary layer mixing scheme. Part I: Scheme description and single-column model tests. *Mon. Wea. Rev.*, **128**, 3187–3199, doi:10.1175/1520-0493(2000)128<3187:ANBLMS>2.0.CO;2; Corrigendum, **129**, 905–905, doi:10.1175/1520-0493(2001)129<0905:C>2.0.CO;2.

Lothon, M., D. H. Lenschow, D. Leon, and G. Vali, 2005: Turbulence measurements in marine stratocumulus with airborne Doppler radar. *Quart. J. Roy. Meteor. Soc.*, **131**, 2063–2080, doi:10.1256/qj.04.131.

Malinowski, S. P., and Coauthors, 2013: Physics of Stratocumulus Top (POST): Turbulence mixing across the capping inversion. *Atmos. Chem. Phys.*, **13**, 12 171–12 186, doi:10.5194/acp-13-12171-2013.

Mather, J. H., and J. W. Voyles, 2013: The ARM Climate Research Facility: A review of structure and capabilities. *Bull. Amer. Meteor. Soc.*, **94**, 377–392, doi:10.1175/BAMS-D-11-00218.1.

Mellado, J. P., B. Stevens, and H. Schmidt, 2014: Wind shear and buoyancy reversal at the top of stratocumulus. *J. Atmos. Sci.*, **71**, 1040–1057, doi:10.1175/JAS-D-13-0189.1.

Moran, K. P., B. E. Martner, M. J. Post, R. A. Kropfli, D. C. Welsh, and K. B. Widener, 1998: An unattended cloud-profiling radar for use in climate research. *Bull. Amer. Meteor. Soc.*, **79**, 443–455, doi:10.1175/1520-0477(1998)079<0443:AUCPRF>2.0.CO;2.

Nicholls, S., 1984: The dynamics of stratocumulus: Aircraft observations and comparisons with a mixed layer model. *Quart. J. Roy. Meteor. Soc.*, **110**, 783–820, doi:10.1002/qj.49711046603.

——, and J. D. Turton, 1986: An observational study of the structure of stratiform cloud sheets: Part II. Entrainment. *Quart. J. Roy. Meteor. Soc.*, **112**, 461–480, doi:10.1002/qj.49711247210.

Stevens, B., and Coauthors, 2003: On entrainment rates in nocturnal marine stratocumulus. *Quart. J. Roy. Meteor. Soc.*, **129**, 3469–3493, doi:10.1256/qj.02.202.

Tennekes, H., 1970: Free convection in the turbulent Ekman layer of the atmosphere. *J. Atmos. Sci.*, **27**, 1027–1034, doi:10.1175/1520-0469(1970)027<1027:FCITTE>2.0.CO;2.

——, 1973: A model of the dynamics of an inversion above the convective boundary layer. *J. Atmos. Sci.*, **30**, 558–567, doi:10.1175/1520-0469(1973)030<0558:AMFTDO>2.0.CO;2.

——, and A. G. M. Driedonks, 1981: Basic entrainment equations for the atmospheric boundary layer. *Bound.-Layer Meteor.*, **20**, 515–531, doi:10.1007/BF00122299.

Wang, S., J.-C. Golaz, and Q. Wang, 2008: Effect of intense wind shear across the inversion on stratocumulus. *Geophys. Res. Lett.*, **35**, L15814, doi:10.1029/2008GL033865.

Wood, R., 2012: Stratocumulus clouds. *Mon. Wea. Rev.*, **140**, 2373–2423, doi:10.1175/MWR-D-11-00121.1.

Zeman, O., and H. Tennekes, 1977: Parameterization of the turbulent energy budget at the top of the daytime atmospheric boundary layer. *J. Atmos. Sci.*, **34**, 111–123, doi:10.1175/1520-0469(1977)034<0111:POTTEB>2.0.CO;2.

Zhang, M. H., and J. L. Lin, 1997: Constrained variational analysis of sounding data based on column-integrated conservations of mass, heat, moisture, and momentum: Approach and application to ARM measurements. *J. Atmos. Sci.*, **54**, 1503–1524, doi:10.1175/1520-0469(1997)054<1503:CVAOSD>2.0.CO;2.

——, ——, R. T. Cederwall, J. J. Yio, and S. C. Xie, 2001: Objective analysis of ARM IOP data: Method and sensitivity. *Mon. Wea. Rev.*, **129**, 295–311, doi:10.1175/1520-0493(2001)129<0295:OAOAID>2.0.CO;2.

Zhu, P., B. A. Albrecht, V. P. Ghate, and Z.-D. Zhu, 2010: Multiple scale simulations of stratocumulus clouds. *J. Geophys. Res.*, **115**, D23201, doi:10.1029/2010JD014400.